Conical Moving-Bed Shale Retort Model

This two-dimensional model of a moving-bed shale oil retort accounts for the major physical interactions of convective heating and kerogen decomposition coupled with the shale and gas flow distributions. Data in a small-sale apparatus support a solids flow model of potential flow, although the exiting boundary conditions are uncertain. The calculations show that efficient retorting will only occur if the upper shale surface is shaped so that the shale particle velocity is perpendicular to this surface, and parallel to the entering retort gas flow. Even in the ideal flow case, performance is quite sensitive to gas/solids flow ratio. This model could be used with measured temperature distributions to optimize the surface profile.

David H. Anderson
Ajit V. Sapre
Clinton R. Kennedy
Frederick J. Krambeck
Mobil Research and Development Corporation
Paulsboro Research Laboratory
Paulsboro, NJ 08066

Introduction

The aboveground processing of oil shale in a solids upflow moving-bed retort was initially patented in 1950 by Berg. Figure 1 shows the design of the retorting apparatus. Cool shale, crushed to about 2 cm nominal diameter, is pumped up through the bottom of the retort, heated, retorted, and disposed of as the shale falls off the top. The inverted conical design of the bed serves to reduce the internal friction of pumping the upflowing shale. Retorted shale piles up on top of the bed at its natural angle of repose. Hot gas, flowing counter to the moving shale bed, enters through the top of the bed and provides the heat for retorting and preheating the rock to reaction conditions, and carries off the product oil vapors. The product vapors cool and condense to a mist, then coalesce to a liquid stream as they pass through the lower portions of the bed. Finally, a mix of gas, mist, and liquid exits through disengaging slots at the bottom of the bed.

In the original design of the inventors, air was used to combust residual coke on the spent shale at the top of the conical vessel. Retorting occurred below the combustion zone as the hot combustion product gases heated the incoming shale rock to liberate oil through kerogen decomposition. A subsequent preferred design that excluded combustion in the vessel was introduced (Duir et al., 1983) in which part of the gaseous product of retorting is recycled and indirectly heated to about 810 K to serve as the hot retort gas. In this design, the retorting zone (670–810 K) would be at the top of the bed. It was found that retorting too deep in the bed caused agglomeration of shale particles due to the weight of the shale. The indirectly heated retort was designed to allow processing of 135 kg/s of shale rock with a liquid yield of 1.4×10^{-4} m^3/kg shale.

In the present analysis, we have formulated an approximate two-dimensional, axially symmetric steady-state mathematical model of the indirectly heated retort to investigate the shale and recycle gas flow patterns and their influence on shale heatup and kerogen conversion. Our approach includes the major physical interactions occurring in a conical moving-bed shale retort, although the complexity and details are approximate in this first model of the process. Because of the conical configuration, the recycle gas flows nonuniformly through the bed, preferring flow near the wall rather than at the center. Data obtained in our laboratory on the upflow pattern of granules in a small-scale conical apparatus suggest that the solids follow a potential flow model, although the exact outlet boundary conditions are uncertain. Simulations with various boundary conditions show that efficient retorting is only achieved if the solids exit velocity is perpendicular to the upper shape surface, thus directly opposite the gas velocity there. Depending on the flow pattern followed by the shale, the upper surface can be scraped to a contour that accomplishes this. If temperature distribution data were available, the model could be used to estimate the solids flow pattern near the shale surface and then determine an optimum surface profile.

It was also found that retort performance is quite sensitive to gas/solids flow ratio. Too high a ratio causes high temperatures deep in the shale bed, which can cause particle agglomeration. Too low a ratio results in incomplete shale conversion.

Model

The geometry of the conical retort shown in Figure 1 reflects the basic features reported by Duir et al. (1983). The retort shell has a lower cone with walls slightly less steep than the upper cone. Shale is fed in the large-scale unit with a 3.05 m dia. piston. Other dimensions used in our simulation are scaled to this piston diameter and the configuration shown by Duir et al. The pile of shale on top slopes with an assumed angle of repose of

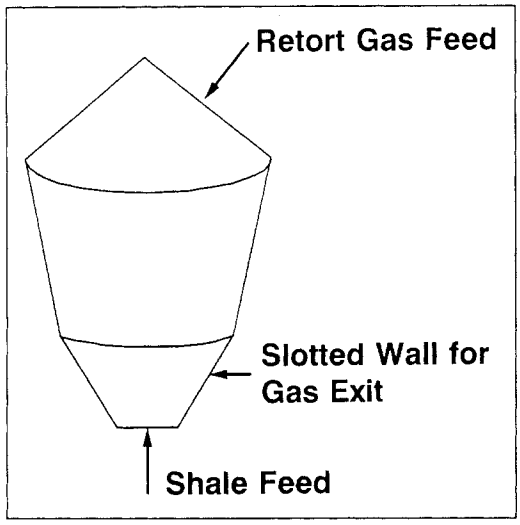

Figure 1. Conical moving-bed shale retort.

38°. The boundaries of the present two-dimensional model (cylindrically symmetrical about the retort centerline) are shown in Figure 2. Retort gas exit slots are located on the lower cone. An oil seal prevents gas flow through the base of the retort.

The model includes a description of gas and solids flow along the interphase heat transfer and kerogen decomposition. Several simplifications and assumptions have been made in formulating the model. These include:

- Bed voidage and shale size are uniform
- Mass depletion of shale due to retorting (~10 wt. %) is neglected
- Additional gas flow from vaporized shale oil is neglected
- Condensed liquid oil flow is neglected
- Enthalpies of retorting, vaporization, or condensation are neglected in comparison to sensible heat transfer
- Heat conduction in each phase is negligible
- Intraparticle temperature gradients are neglected

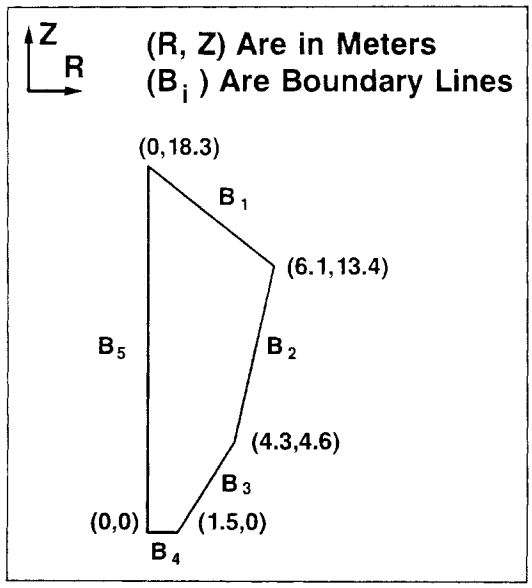

Figure 2. Two-dimensional model boundaries.

- Constant gas and solid heat capacities
- All physical properties are independent of variation in composition
- Raw shale has uniform kerogen content

Our results show sensitivity of the retorting performance to shale temperature profiles determined by the flow distribution of gas and shale and their countercurrent heat exchange. Assessment of the magnitude of the sensitivity to unbalanced flow may be improved later by including some of the complexity we have neglected. With these assumptions, conservation of mass in each phase is then given by

$$\nabla \cdot \boldsymbol{G} = \frac{1}{r}\frac{\partial}{\partial r} r G_r + \frac{\partial}{\partial z} G_z = 0 \tag{1}$$

$$\nabla \cdot \boldsymbol{S} = 0 \tag{2}$$

$\boldsymbol{G}$ and $\boldsymbol{S}$ are the gas and shale mass velocity vectors, respectively. Subscripts r and z indicate radial and axial components, respectively.

Only convective heat transfer effects are included in the model. The heat balances within the retort are then

$$C_{pg}(\boldsymbol{G} \cdot \nabla T_g) = C_{pg}\left(G_r \frac{\partial T_g}{\partial r} + G_z \frac{\partial T_g}{\partial z}\right) = (hA)_m (T_s - T_g) \tag{3}$$

$$C_{ps}(\boldsymbol{S} \cdot \nabla T_s) = (hA)_m (T_g - T_s) \tag{4}$$

with boundary conditions of entering gas and shale solid temperatures; that is,

$$T_s = T_{so} \quad \text{on} \quad B_4 \tag{5}$$

$$T_g = T_{go} \quad \text{on} \quad B_1 \tag{6}$$

$(hA)_m$ is the product of the convective heat transfer coefficient with the interfacial area based on the average particle size (assumed 0.02 m) of the process. The heat transfer coefficient is a function of the local gas velocity, but these calculations do not depend on the kerogen decomposition profiles, which may thus be determined independently once the temperature and velocity profiles are calculated.

Retorting kinetics are complex in terms of product distributions (Wallman et al., 1981), but the overall kerogen decomposition rate is approximated as first order in the kerogen weight fraction with Arrhenius temperature dependence (Mobil lab data by E. F. Kondis). The kerogen balance for particles in the moving bed system is, based on these kinetics,

$$\boldsymbol{S} \cdot \nabla F = -\rho_s (1 - \epsilon) k_o \exp(-E/RT_s) F \tag{7}$$

where F is the fraction of initial kerogen remaining in the particle and $(1 - F)$ is the conversion. The raw shale is assumed to have uniform kerogen content, so $F = 1$ at the retort bottom ($z = 0$).

Gas flow

As described by Stanek and Szekely (1974), the gas flow pattern in a packed bed is determined by applying Ergun's

equation locally in the direction of flow. The vectorial form of the Ergun equation is

$$-\nabla P = V(f_1 + f_2 V) \tag{8}$$

where P is the pressure and V the fluid velocity vector. The parameters f_1 and f_2 are

$$f_1 = 150\mu\,(1-\epsilon)^2/D_p^2\epsilon^3 \tag{9a}$$

$$f_2 = 1.75\rho\,(1-\epsilon)/D_p\epsilon^3 \tag{9b}$$

Direct reference to the pressure field can be eliminated in terms of the fluid mass velocity for a compressible gas that obeys the ideal gas law. Then

$$\rho = \frac{PM}{RT} \tag{10}$$

and Eq. 8 is converted to

$$-\tfrac{1}{2}\nabla P^2 = G\hat{f} \tag{11}$$

where

$$\hat{f} = f_1 P/\rho + f_2 G P/\rho^2 \tag{12a}$$

and G is the magnitude of the gas velocity

$$G = [(G_r)^2 + (G_z)^2]^{1/2} \tag{12b}$$

Note that from Eqs. 9 and 10, the pressure dependencies cancel out in Eq. 12a. Taking the curl of Eq. 11 gives

$$\nabla \times G - G \times \nabla \ln \hat{f} = 0 \tag{13}$$

which is independent of pressure.

The gas flow solution is most clearly displayed in terms of stream function, ψ, where

$$G_r = -\frac{1}{r}\frac{\partial \psi}{\partial z}$$

$$G_z = \frac{1}{r}\frac{\partial \psi}{\partial r} \tag{14}$$

Equation 14 automatically satisfies mass continuity, Eq. 1. Only the θ component of Eq. 13 is of interest, and with the use of Eqs. 14 this becomes:

$$\frac{\partial^2 \psi}{\partial z^2} + \frac{\partial^2 \psi}{\partial r^2} - \frac{1}{r}\frac{\partial \psi}{\partial r} = -\frac{\partial \psi}{\partial z}\frac{\partial \ln \hat{f}}{\partial z} - \frac{\partial \psi}{\partial r}\frac{\partial \ln \hat{f}}{\partial r} \tag{15}$$

with

$$G = \frac{1}{r}\left[\left(\frac{\partial \psi}{\partial r}\right)^2 + \left(\frac{\partial \psi}{\partial z}\right)^2\right]^{1/2} \tag{16}$$

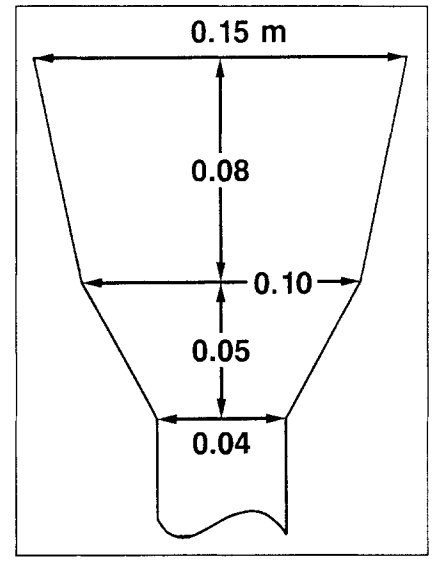

Figure 3. Cold flow scale model dimensions.

Boundary conditions

There is no flow across boundaries B_2, B_4, B_5, Figure 2, which means they are streamlines with constant values of ψ. Because all gas enters at B_1 and exits across B_3, the streamline definition gives at steady state

$$\psi(B_2) = \psi(B_5) - m_g/2\pi \tag{17}$$

in cylindrical geometry, where m_g is the total gas mass flow rate. We set

$$\psi(B_4) = \psi(B_5) = 0 \tag{18}$$

as the reference streamline. Since pressure is uniform along boundaries B_1 and B_3, the gas velocity will be normal (perpendicular) to these faces. In terms of the stream function,

$$\sin\theta_1 \frac{\partial \psi}{\partial r} - \cos\theta_1 \frac{\partial \psi}{\partial z} = 0 \quad \text{on} \quad B_1 \tag{19}$$

$$\sin\theta_3 \frac{\partial \psi}{\partial r} - \cos\theta_3 \frac{\partial \psi}{\partial z} = 0 \quad \text{on} \quad B_3 \tag{20}$$

where θ_i is the angle between the boundary and the horizontal direction.

Solids flow

To determine the shale flow patterns, a small-scale cold flow experimental program was performed in our laboratory. Tracer experiments were conducted in a glass scale model that approximated the full-scale configuration, as shown in Figure 3. 1–2 mm gravel was fed from the bottom with a piston feeder analogous to the actual feed device. A pistonful was fed to the vessel, then another, and so on. Flow visualization was effectively accomplished by alternately injecting different colored gravel until a steady-state layered bed pattern was attained. Subsequent removal and measurement of the layers provided a quantitative picture of the flow.

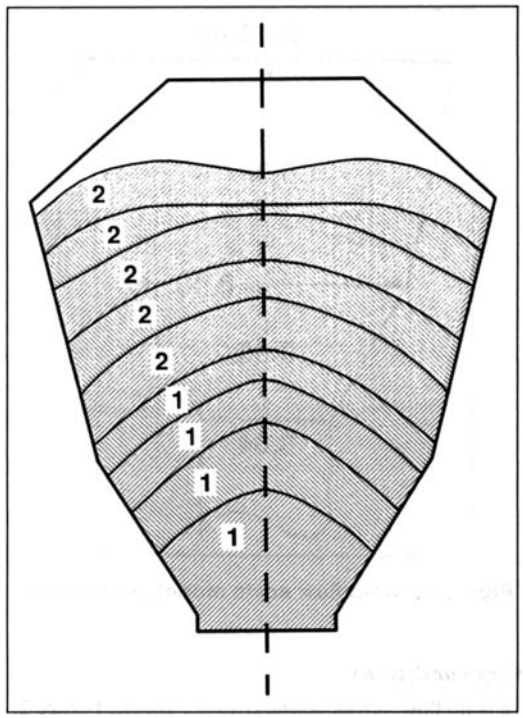

Figure 4. Cold flow data—layered bed pattern.

The two-dimensional results are shown in Figure 4; the numbers indicate the relative volumes of the layers. In a system continuously fed at a constant rate, these fronts would correspond to positions at similarly specified time intervals. Note that the flow rate appears uniform along the fronts until the vicinity of the pile, where there is a slowing in the center compensated by an increasing rate at the walls. The fronts in the pile region were difficult to measure, however, so the picture is only qualitative there. Movement of the particles was generally away from the centerline toward the pile surface before exiting. Material in the center had the longest residence time as its path to the exit was longest. The region at the top evidenced little or no replacement of particles. In summary, exit was toward the sloping sides of the pile. There was no direct short-circuiting in the bed, nor was there a completely dead zone aside from the very top.

The angles of internal friction and repose of the gravel used in the cold flow study are not precisely those of shale, however. Also, the impact of oil percolating through the bed as would occur during retorting is not included. For these reasons, the cold flow results should be considered as an initial approximation of shale flow in the retort.

Approximate solids flow model

The flow behavior observed in the small-scale model is similar to the nature of downward flowing granules in wedge-shaped hoppers. In cases where all material is mobilized in a hopper, radial flow typically exists apart from regions near the entrance and exit of the hopper (Kaza and Jackson, 1984). That is, the granules follow paths toward the exit rather than flowing vertically. Our approximation of the flow of solids based on the cold flow studies is ideal, irrotational flow described by

$$\frac{\partial S_r}{\partial z} - \frac{\partial S_z}{\partial r} = 0 \tag{21}$$

as the equation of motion. Defining the shale stream function, ψ_s, by

$$S_r = -\frac{1}{r}\frac{\partial \psi_s}{\partial z}$$

$$S_r = \frac{1}{r}\frac{\partial \psi_s}{\partial z} \tag{22}$$

which satisfies the shale mass balance, Eq. 2, gives

$$\frac{\partial^2 \psi_s}{\partial z^2} + \frac{\partial^2 \psi_s}{\partial r^2} - \frac{1}{r}\frac{\partial \psi_s}{\partial r} = 0 \tag{23}$$

Boundary conditions

On specifying a vertical entrance to the bed ($z = 0$),

$$\frac{\partial \psi_s}{\partial z} = 0; \quad z = 0 \tag{24}$$

The centerline ($r = 0$) is a streamline in cylindrical symmetry. It is specified as the reference streamline; that is,

$$\psi_s = 0; \quad r = 0 \tag{25}$$

As in gas flow, Eq. 18,

$$\psi_s = m_s/2\pi \tag{26}$$

along the retort wall where m_s is the total shale mass flow rate.

Shale velocity at the slanted face of the pile, B_1, is initially assumed to be normal to that face.

$$\sin\theta_1 \frac{\partial \psi_s}{\partial r} - \cos\theta_1 \frac{\partial \psi_s}{\partial z} = 0 \quad \text{on} \quad B_1 \tag{27}$$

The sensitivity of the results to this assumption are discussed later.

Computational Procedure

The equations of gas and shale flow patterns and temperatures along with the kerogen conversion were solved numerically using the method of finite differences. Table 1 shows constant physical property parameters used in the calculations.

The high value of the gas phase heat capacity results from its high hydrogen plus hydrocarbon content, ~75 mol %, as in Duir

Table 1. Physical Properties

C_{pg}	2.26 J/g · K
C_{ps}	1.15 J/g · K
m_s	135 kg/s
ρ_s	1,920 kg/m^3
ϵ	0.4
D_p	0.02 m (avg. of typical distribution)
M_w	27 (recycle gas)
E	180 kJ/gmol
k_o	2.2 × 10^{10}/s

et al. The shale flow rate is assumed to be 135 kg/s, as in Duir et al. Sensitivity to gas flow rate is discussed later. The retorting kinetic rate constants were determined in our laboratory for particles of this size.

Gas viscosity, μ, was estimated over a 300–810 K range to be

$$\mu\,(\text{Pa}\cdot\text{s}) = -2.41\times10^{-6} - 3.55\times10^{-8}\,T_g - 1.17\times10^{-11}\,T_g^2 \quad (28)$$

Additional sensitivity to gas-solid contacting efficiency will derive from the dependence of the convective heat transfer coefficient on the local gas velocity. We used the following standard correlation (Bird et al., 1960).

$$h = C_{pg}\,G\,j_H\left(\frac{C_{pg}\mu}{k_g}\right)^{-2/3} \quad (29)$$

k_g is the gas conductivity taken constant at 0.035 W/m · K and

$$j_H = \begin{cases} 0.91\,\text{Re}^{-0.51}\beta & \text{Re} < 50 \\ 0.61\,\text{Re}^{-0.41}\beta & \text{Re} > 50 \end{cases} \quad (30)$$

$$\text{Re} = \frac{G}{A\mu\beta} \quad (31)$$

β is the particle sphericity, assumed to be 0.86. The interfacial area per unit volume is 180 m^{-1}. Inlet temperatures for the shale and gas were set at 370 and 810 K, respectively.

Results and Discussion

Figure 5a is a contour plot of constant values of the solids flow stream function, that is, streamlines. On each side of the centerline, 10% of the total mass rate of solids flows between consecutive streamlines. The results show the vertical entrance followed by a rapid approach to radial flow. Because of our boundary conditions at the top, the flow deviates toward the pile surface, but only very near the pile itself, as observed similarly in the cold flow studies. Figure 5b shows the position of the fronts (particles entering at the same time) at constant time intervals up the retort, and may be compared with the cold flow picture. The similarity below the pile is good and the crowding of these fronts at the top indicates the gradual slowing of the shale flow; therefore, our approximate solids flow equations reasonably describe the flow behavior, although there may be significant errors in the critical region near the surface.

The solids flow velocities were incorporated into the complete retort model. Initially, the gas flow rate was chosen to satisfy $m_g \cdot C_{pg} = m_s\,C_{ps}$; that is, balanced thermal mass flow rates. This condition gives $m_g = 68$ kg/s. Recycle gas 10% streamlines in Figure 6a show the preferential gas flow toward the edge of the vessel as a result of the flow resistance of the pile.

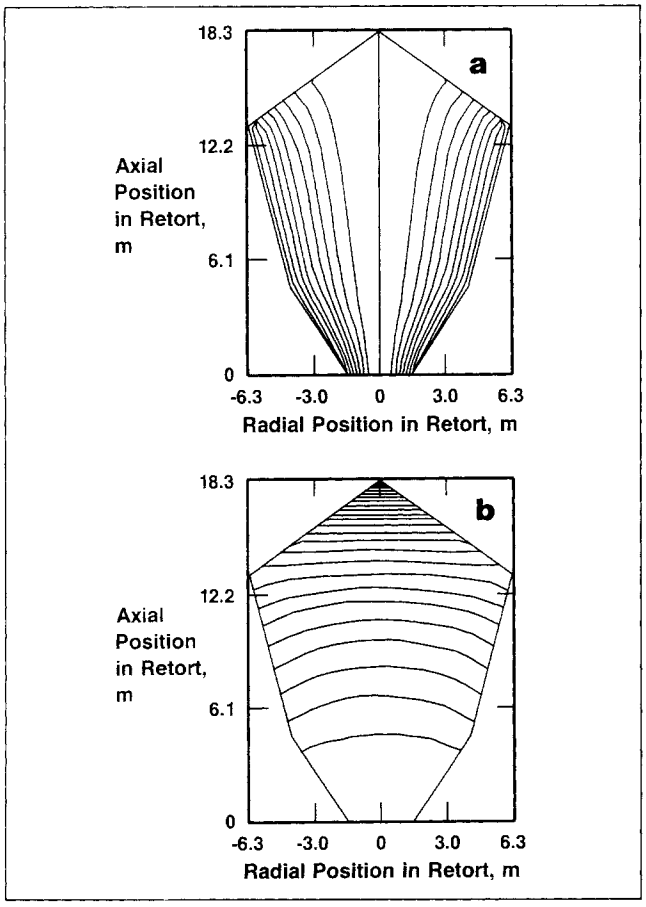

Figure 5. Shale flow model results.
(a) Shale streamlines
(b) Shale position at constant time intervals

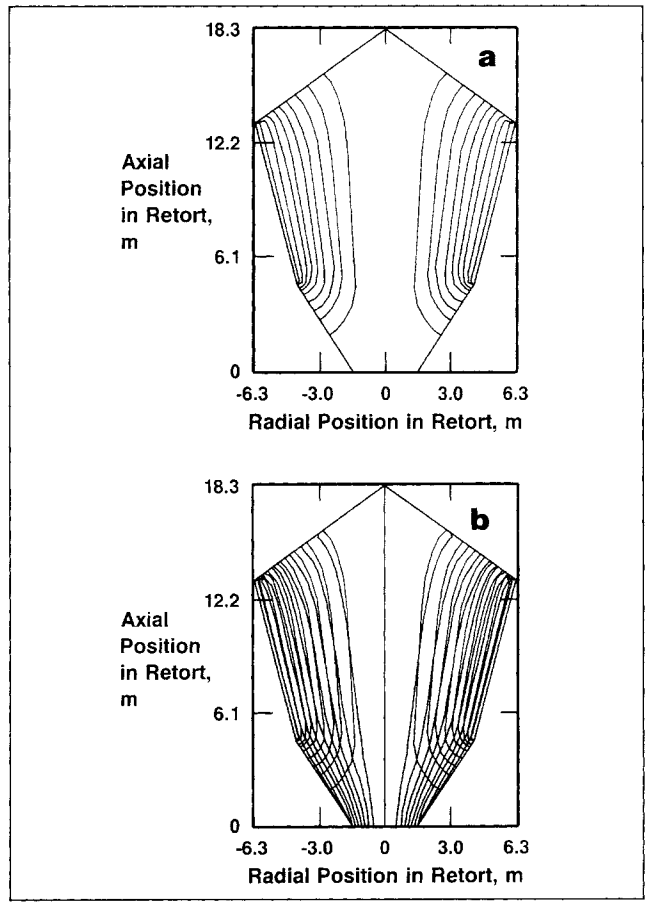

Figure 6. Streamlines.
(a) Recycle gas
(b) Shale and gas

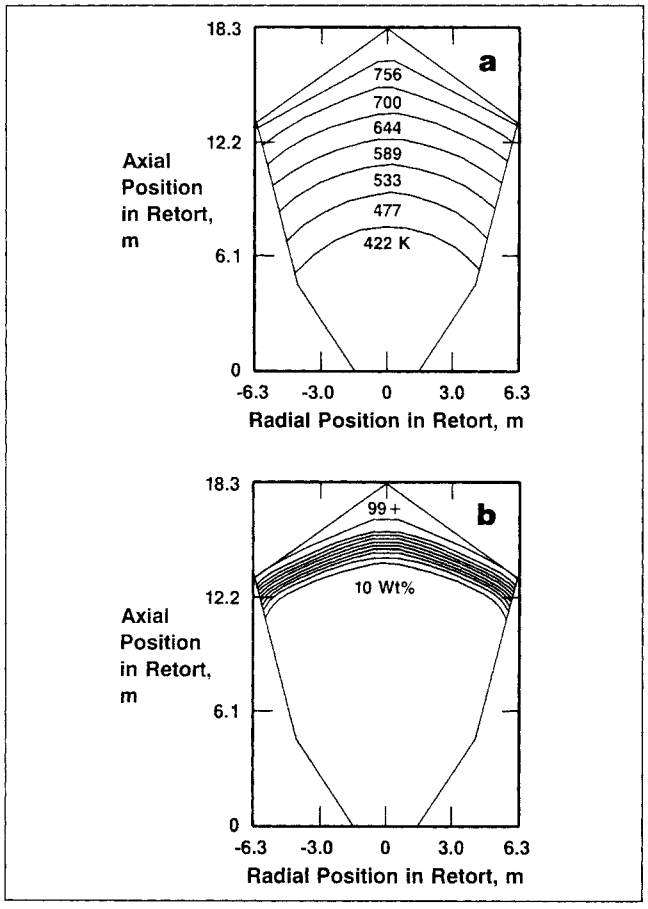

Figure 7. Balanced gas and shale flow rates.
(a) Shale isotherms
(b) Kerogen conversion

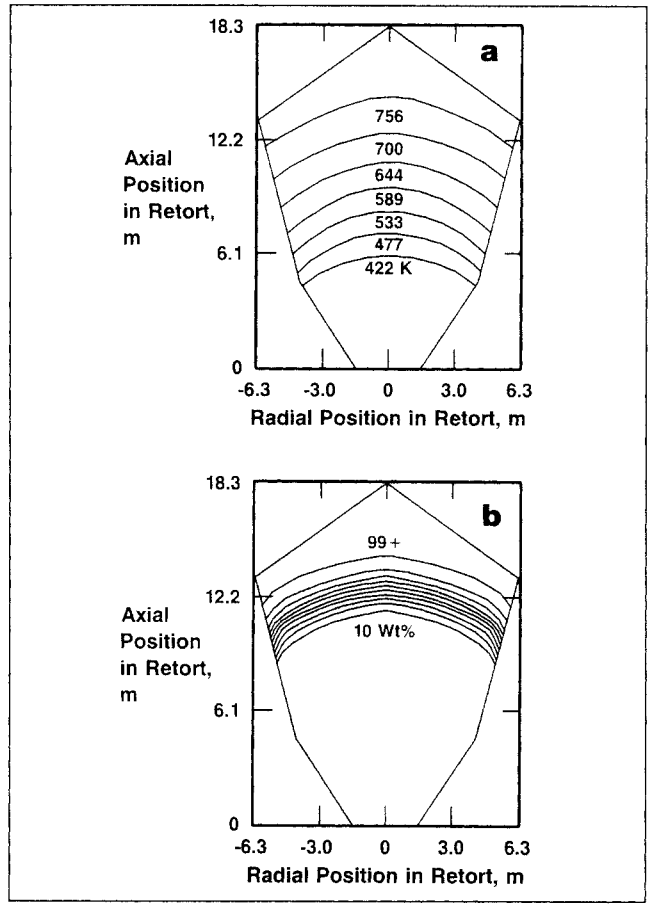

Figure 8. 10% excess gas flow rate.
(a) Shale isotherms
(b) Kerogen conversion

Figure 6b shows that in spite of this nonuniform gas flow, the gas and shale streamlines are similar under the assumption of solids flow perpendicular to the surface. As a result, the shale isotherms, Figure 7a, and kerogen conversion contours, Figure 7b, are parallel to the pile surface. Most conversion occurs in or near the pile, and the model predicts overall complete conversion with the present parameters. However, as is shown later, this result is very sensitive to the assumed flow direction of the shale at the top surface. The good performance prediction depends entirely on the assumption that the shale flows normal to the surface, or in other words, parallel to the gas flow.

Increasing the gas flow rate by 10% shows the sensitivity of the retort to deviation from balanced gas/solid contacting. The shale streamlines are as before. Also, the 10% gas flow streamlines do not change significantly, so the gas velocity at any point increases by 10% relative to the first case. The bed temperature has increased above the exit slots, Figure 8a, because of the gas flow increase. Complete retorting is achieved in this case also, Figure 8b, but occurs below the pile now. We have no information on how low in the bed retorting can take place without leading to particle agglomeration. The present model cannot show the dynamical effects of gas flow bypassing resulting from agglomeration, but the evident sensitivity of the temperature profiles to local changes in gas to solid flow rates suggests a potential for operational problems.

In the case where overall gas flow is 10% less than the first case, the bed temperature drops, Figure 9a, and kerogen decomposition occurs only just before the shale exits, Figure 9b. Overall conversion falls to about 80%. Additional yield loss through carryover of product with the spent shale may be expected.

Given the model assumptions and the shale flow pattern shown in Figure 5a, good retort performance is expected within a narrow range of operating conditions of overall gas to shale flow ratio. Still unknown, however, is the actual shale flow pattern in the pile region where most retorting should occur. The pile geometry determines the gas flow pattern in this region. Any major difference in the shale flow there from the previous description would jeopardize the local balance of gas and shale thermal mass fluxes even when balanced overall.

As an example, suppose the shale were to flow vertically at the exit while the pile shape remained the same. Using this boundary condition,

$$\frac{d\psi_s}{dz} = 0 \quad \text{on} \quad B_1 \tag{32}$$

instead of condition Eq. 27 leads to the solution for the shale flow shown in Figure 10a for the positions at constant time intervals. Here the flow is essentially uniform radially everywhere, as

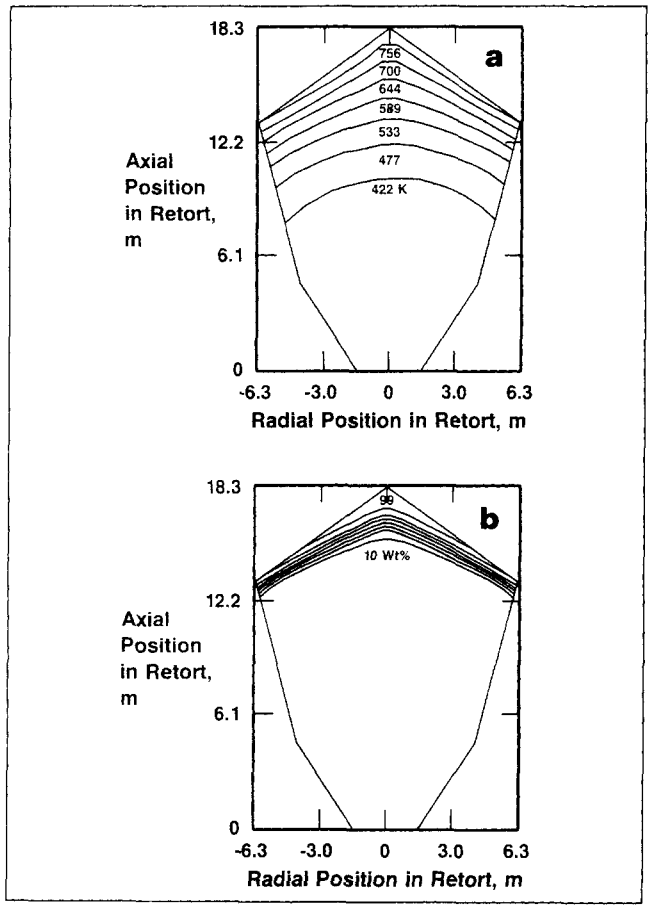

Figure 9. 10% reduced gas flow rate
(a) Shale isotherms
(b) Kerogen conversion

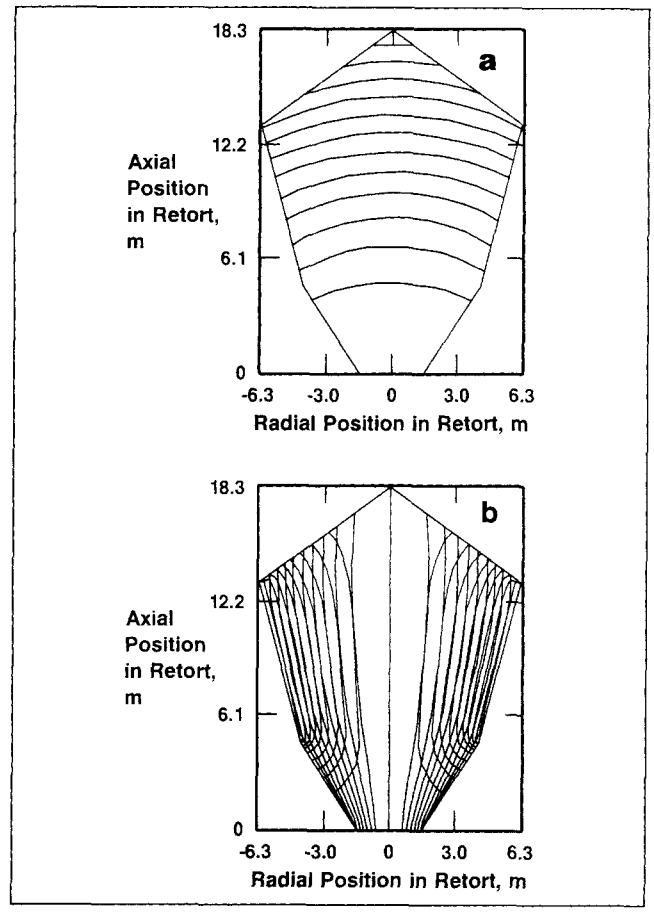

Figure 10. Vertical shale flow exit boundary condition.
(a) Shale position at constant time intervals
(b) Shale and gas streamlines

these fronts are parallel to each other with no slowing seen in the pile. Figure 10b compares the 10% shale streamlines for this case with those of the retort gas at $m_g = 68$ kg/s. While in overall balance of gas and shale thermal mass flow rates, the decreasing gas flux in the pile away from the retort edge is not reflected by the shale flow. As a result, high temperature penetrates far into the bed near the wall, Figure 11a, while the center region is not heated sufficiently, allowing unretorted shale to exit, Figure 11b. The overall yield loss is about 5%. With dissimilar flow patterns of gas and shale, both reduced yield and potential particle agglomerating conditions may occur with a single gas to shale flow ratio. Even without this degree of difference between their flow patterns, gas to shale flow nonuniformity apparently would reduce the operable range of overall recycle gas rate.

A possible means of improving the retorting performance if the shale flow pattern were vertical at its exit would be to scrape off the pile. Scraping the entire pile would result in shale flow normal to exiting surface and parallel to the gas flow. We computed the model solution on removing the whole pile. Over the resulting flat boundary, the gas flow boundary condition becomes

$$\frac{d\psi}{dz} = 0 \tag{33}$$

Figure 12 shows the gas and solid streamlines for this case and it is clear that they match with each other in the critical region near the top where most retorting occurs. The shale isotherms are plotted in Figure 13a. These isotherms are almost parallel to the exiting surface, and more uniform than those shown in Figure 11a. Figure 13b shows the improved kerogen conversion in the center of the bed for this case with $m_g = 68$ kg/s. No yield loss is observed.

The above examples illustrate the importance of matching the gas and shale flow patterns in order to achieve efficient retorting. Most important is gas and solids streamlines in the exiting pile region. We suggest that the pile should be scraped such that shale exits perpendicular to the exit boundary. In our model, this resulted in parallel gas and solids streamlines. However, solids flow behavior in the exit region should be accurately known to devise proper scraping strategy. The gas/solids flow patterns in a commercial retort could be determined from the temperature profiles obtained during retorting, and operating problems minimized by properly scraping the shale pile.

Conclusions

Our two-dimensional model of the conical oil shale moving-bed retort shows:

1. The upward flow pattern of solids observed in experimental

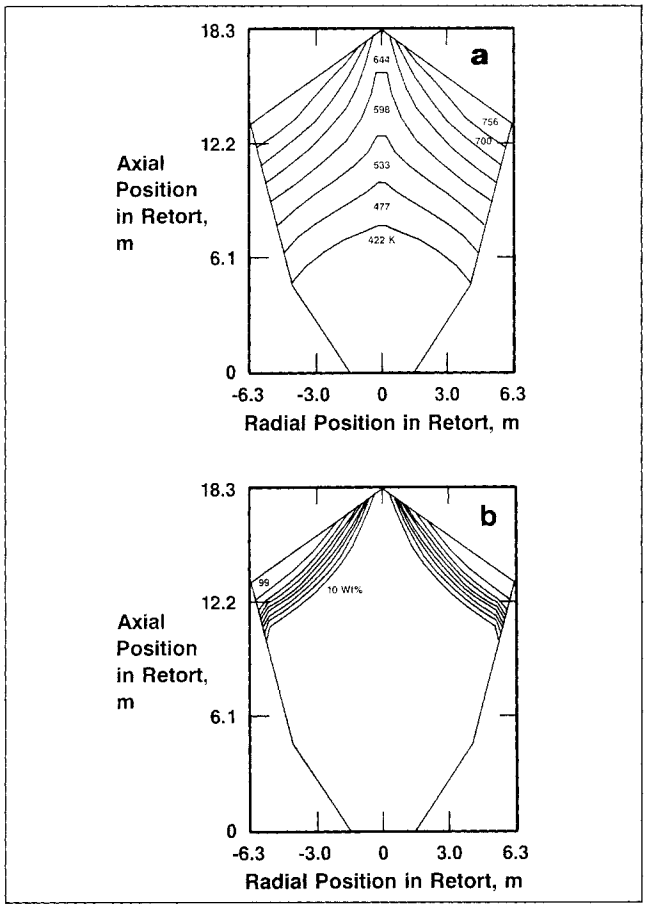

Figure 11. Retort performance based on the condition of Figure 10.
(a) Shale isotherms
(b) Kerogen conversion

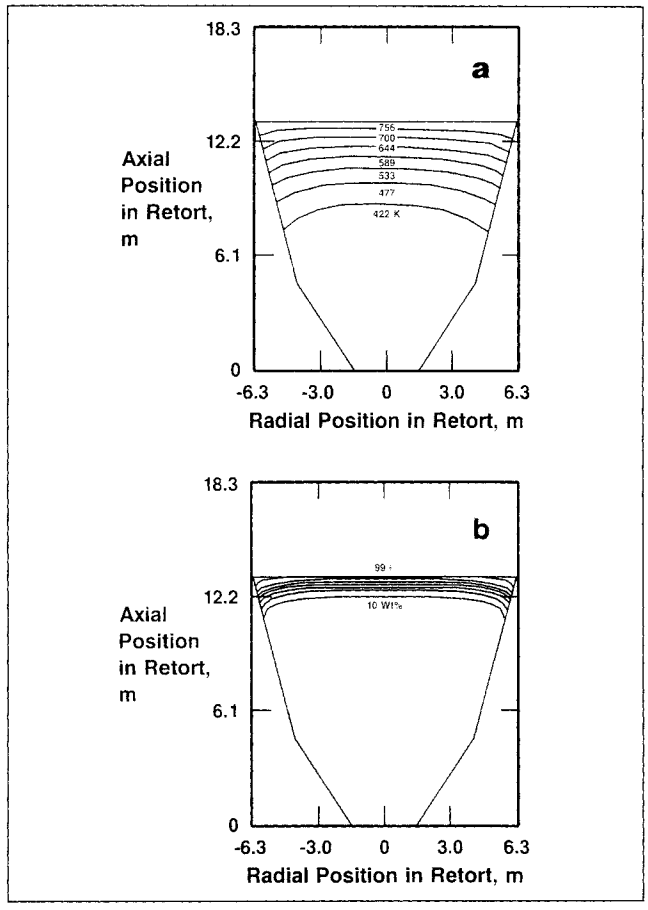

Figure 13. Retort performance based on the condition of Figure 12.
(a) Shale isotherms
(b) Kerogen conversion

cold flow studies is reasonably described by the potential flow assumption, indicating uniform flow within the vessel boundaries. The exact behavior in the critical upper surface region is uncertain, however.

2. The overall oil yield is sensitive to gas and solids flow patterns in the region near the top of the retort where most of the conversion takes place. For the best retorting performance, it is critical to match gas/solids streamlines in this region.

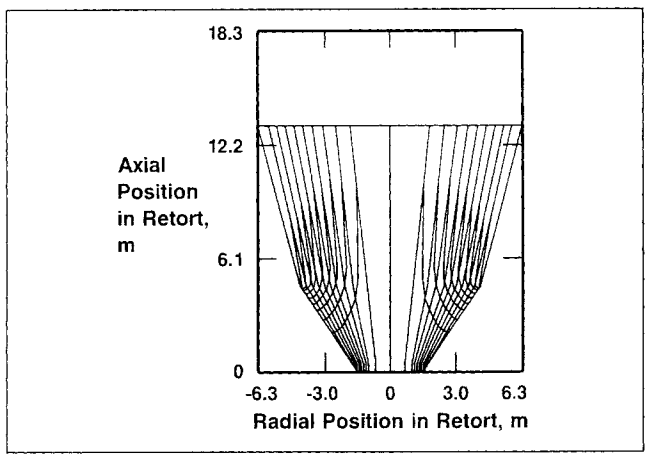

Figure 12. Shale and gas streamlines with the pile removed.

3. To achieve balanced parallel gas/solids streamlines in the pile region, we recommend scraping the pile such that exiting shale particles flow perpendicular to the exit boundary.

4. Even with ideal flow patterns, the performance is very sensitive to gas/solids flow ratio. High gas flow could lead to high temperatures too deep in the bed, resulting in particle agglomeration. Alternatively, low gas flow will lead to incomplete retorting and inefficient retort performance.

5. Temperature profile measurements in an existing unit could be used with the model to back out the solids flow pattern near the surface. This could then be used to determine the optimum surface profile.

Sensitivity of calculated retort performance was largely dependent on resulting temperature profiles. These profiles and the performance were primarily affected by a deviation from balanced countercurrent flow of gas and shale. The magnitude of sensitivity of the temperature profiles to flow maldistribution may be determined more accurately in more refined models by including effects such as enthalpy of kerogen decomposition or mass transfer from the shale to the vapor phase.

Acknowledgment

We wish to acknowledge the support of the Paulsboro Research Laboratory of Mobil R&D Corporation. J. H. Beech and Q. N. Le developed the solids flow scale model study. The kinetic data were determined by E. F. Kondis.

Notation

A = interfacial area
C_{ps}, C_{pg} = shale and gas specific heat capacities
D_p = averge particle diameter
E = activation energy for kerogen decomposition
f_1, f_2 = Ergun coefficients
f = term in Eq. 12
F = fraction of kerogen remaining
g, g_c = gravitational constant and conversion factor
G, G_r, G_z = gas mass velocity and components
G = magnitude of gas velocity
h = gas/particle convective heat transfer coefficient
k_g = gas phase conductivity
k_o = kerogen decomposition preexponential factor
m = mass flow rate
M = recycle gas molecular weight
P = pressure
r = radial dimension
R = gas constant
S, S_r, S_z = shale mass velocity and components
T_g, T_s = retort gas and shale temperature
$\vec{V}, V$ = velocity vector and magnitude
z = axial dimension

Greek letters

β = sphericity
ϵ = bed voidage
σ = normal stress
θ = angle of retort boundaries
ψ = stream function
ρ = density
μ = viscosity

Subscripts

r, z = radial, axial components
g, s = value for gas, shale

Literature Cited

Berg, C. H. O., U.S. Patent No. 2,501,153, "Shale Oil Eduction," *U.S. Patent and Trademark Office Official Gazette*, **632**(3), 792 (Mar. 21, 1950).

Bird, R. B., W. E. Stewart, and E. N. Lightfoot, *Transport Phenomena*, Wiley, New York, 411 (1960).

Duir, J. H., C. E. Griswold, and B. A. Christolini, "Oil Shale Retorting Technology," *Chem. Eng. Prog.*, **79**(2), 45 (1983).

Kaza, K. R., and R. Jackson, "Boundary Conditions for a Granular Material Flowing out of a Hopper or Bin," *Chem. Eng. Sci.*, **39**, 915 (1984).

Stanek, V., and J. Szekely, "Three-Dimensional Flow of Fluids Through Nonuniform Packed Beds," *AIChE J.*, **20**(5), 974 (1974).

Wallman, P. H., P. W. Tamm, and B. A. Spars, "Oil Shale Retorting Kinetics," *Oil Shale, Tar Sands and Related Materials, ACS Symp. Ser.*, **163**, Ch. 7, Am. Chem. Soc. (1981).

Manuscript received June 21, 1989, and revision received Mar. 19, 1990.